What should be considered when simulating Doppler velocities measured by ground-based weather radars?

Olivier Caumont, Véronique Ducrocq

NOTES AND CORRESPONDENCE

What Should Be Considered When Simulating Doppler Velocities Measured by Ground-Based Weather Radars?

Olivier Caumont and Véronique Ducrocq

CNRM/GAME, Météo-France/CNRS, Toulouse, France

ABSTRACT

A sophisticated and flexible simulator of Doppler velocities measured by ground-based weather radars is appended to a high-resolution nonhydrostatic atmospheric model. Sensitivity experiments are conducted by using different configurations for each of the physical processes that is modeled by the simulator. It is concluded that neglecting the vertical beam broadening effect or the weighting by reflectivities yields errors of the same order on the simulated reflectivities. Neglecting hydrometeor fall speeds has a much smaller impact. It is also shown that neglecting both the beam broadening effect and the weighting by reflectivities yields errors of the same order as occur when only one of these effects is neglected.

1. Introduction

Simulators of Doppler velocities measured by ground-based radars are now widely used in the atmospheric community, especially as observation operators to assimilate radar radial velocities into numerical weather prediction (NWP) models. The main issue related to designing a simulator is to find a trade-off between accuracy and computational efficiency inasmuch as the model sophistication enables it.

At present, most observation operators for radial velocities are relatively basic: wind velocities are projected into the radial direction (e.g., Snyder and Zhang 2003). Sometimes the vertical velocity of falling hydrometeors is included (e.g., Sun and Crook 1997; Qiu et al. 2006). A further refinement consists of weighting the fall speeds by reflectivities (e.g., Wu et al. 2000). Few observation operators model the geometry of the radar beam very accurately, however. Some observation operators model the broadening of the radar beam in the vertical, but they do not account for the fall velocity of hydrometeors and the weighting by reflectivities (e.g., Salonen and Järvinen 2004). In certain Observing Sys-

tem Simulation Experiment (OSSE) studies, such as Xue et al. (2006), the fall speed is assumed to be perfectly accounted for by not including the effect of hydrometeor sedimentation in both the data simulation and assimilation. Such effects, including the reflectivity weighting for terminal velocity, have been introduced in more recent OSSE studies (e.g., Tong and Xue 2008). Sun and Crook (2001) also take into consideration the beam broadening effect in the vertical and the hydrometeor fall speed (without reflectivity weighting). None of these studies includes reflectivity weighting for the wind component of radial velocity, however. Some recent more sophisticated radar emulators do include the reflectivity weighting. For example, both the pulse-based simulator of May et al. (2007) and the time series radar simulator of Cheong et al. (2008) include the reflectivity weighting of both wind and hydrometeor fall speeds.

This short review of existing observation operators for Doppler velocities highlights the need for quantifying errors associated with each of the assumptions that are used to simplify observation operators. In this study, we design a comprehensive and flexible radar simulator that is able to take into account the hydrometeor fall speeds, the weighting of Doppler velocities by reflectivities, and the beam broadening in the vertical direction. The mesoscale nonhydrostatic (Méso-NH) atmospheric model enables the simulation of all

Corresponding author address: Olivier Caumont, CNRM/GMME/Micado, Météo-France, 42 Ave. G. Coriolis, 31057 Toulouse CEDEX 1, France.
E-mail: olivier.caumont@meteo.fr

these processes by providing all necessary parameters. Then sensitivity tests are carried out: by neglecting one of these processes separately, the error made when a simpler simulator is used is quantified.

Section 2 presents the formulation and the validation of the full radar simulator. Section 3 describes the sensitivity experiments used to assess errors associated with each approximation, and section 4 unfolds the results of the sensitivity experiments.

2. The radar simulator

The simulator computes Doppler radial velocities from pressure, temperature, hydrometeor contents, and three-dimensional wind components. It is designed to be coupled to models with horizontal resolutions of typically 2–10 km. Intrinsic radar characteristics such as location, wavelength, beamwidth, and elevation angles are defined by the user. In this study, the radar simulator uses predicted three-dimensional fields from the Méso-NH (Lafore et al. 1998) model. This model has an advanced representation of the water cycle, with five prognostic hydrometeors (cloud water, rainwater, primary ice, snow, and graupel) governed by a bulk microphysics parameterization following Caniaux et al. (1994).

a. Physical formulation

Doppler velocities are simulated using the following expression (Doviak and Zrnić 1993):

$$v_r(\mathbf{r}_0) = \frac{\int_{-\pi}^{\pi} \overline{\eta v_r}(\mathbf{r}) f^4(\theta) \, d\theta}{\int_{-\pi}^{\pi} \eta(\mathbf{r}) f^4(\theta) \, d\theta} \, , \qquad (1)$$

where $\mathbf{r}$ is the vector of length r (m) that links the radar emitting antenna to the current position, $\mathbf{r}_0$ is the vector that links the radar emitting antenna to the center of the resolution volume (i.e., the part of space that contributes most to the returned power), θ is the angle to the beam direction in the vertical plane, f^2 is the antenna's radiation pattern (modeled as a Gaussian function),

$$\eta(\mathbf{r}) = \sum_{j \in \text{type}} \int_0^\infty \sigma_j(D, \mathbf{r}) N_j(D, \mathbf{r}) \, dD$$

is the radar reflectivity (m^{-1}), $\sigma_j(D, \mathbf{r})$ is the backscattering cross section of particles of diameter D for the precipitating hydrometeor type j (m^2), N_j is the hydrometeor size distribution (m^{-4}),

$$\overline{\eta v_r}(\mathbf{r}) = \sum_{j \in \text{type}} \int_0^\infty \sigma_j(D, \mathbf{r}) v_{rj}(D, \mathbf{r}) N_j(D, \mathbf{r}) \, dD \; (s^{-1}),$$

and $v_{rj}(D, \mathbf{r})$ is the projection onto the beam direction of the wind vector u_r and that of the hydrometeor fall speed of particles of diameter D (m) for the precipitating hydrometeor type j (m s^{-1}).

Reflectivities are computed from rainwater, snow, primary ice, and graupel contents, following Caumont et al. (2006). In Eq. (1), Rayleigh scattering and standard beam bending are assumed; attenuation is neglected. Considering the beam broadening in the vertical direction is justified by the fact that the resolution of radar data is typically on the order of 1° (i.e., 1.7 km at a range of 100 km), whereas the model vertical resolution generally ranges from a few tens of meters in the lower atmosphere to a few hundred meters in its upper part. Because the model horizontal resolution is not finer than 2 km, however, beam broadening is not taken into consideration in the horizontal plane. Moreover, effects related to the finite receiver bandwidth are neglected because gate lengths are typically on the order of a few hundred meters, well below the model horizontal resolution.

In this study, the integrals in Eq. (1) that allow one to account for beam broadening are efficiently evaluated by means of a Gauss–Hermite quadrature, following Caumont et al. (2006). For each elevation, three ray paths are computed, whose elevations correspond to the Gauss–Hermite nodes. The model variables at grid points are interpolated onto ray paths by means of a bilinear interpolation.

b. Application to the 23 June 2005 convective case

The quality of the simulator is qualitatively verified for a meteorological case. On 23 June 2005, a cold low pressure area crossed France from west to east. As it moved over warm air, deep convection occurred over northern France. Convective cells began to form over northern France at about 1200 UTC and then grew and merged so as to form a mesoscale convective system that swept across northern France eastward. An atmospheric simulation is conducted with the Méso-NH model starting at 1200 UTC from an Aire Limitée Adaptation Dynamique Développement International (ALADIN) analysis, the French operational limited-area mesoscale NWP system. The model setup is the same as the one used by Ducrocq et al. (2002) for convective cases, except for the two domain locations. The radar simulator is applied to the inner domain outputs for three radars that cover the area (Abbeville, Arcis, and Trappes; see locations in Fig. 1 and characteristics in Table 1).

Doppler velocities are simulated with equations from section 2a without further approximation (Figs. 1c,d).
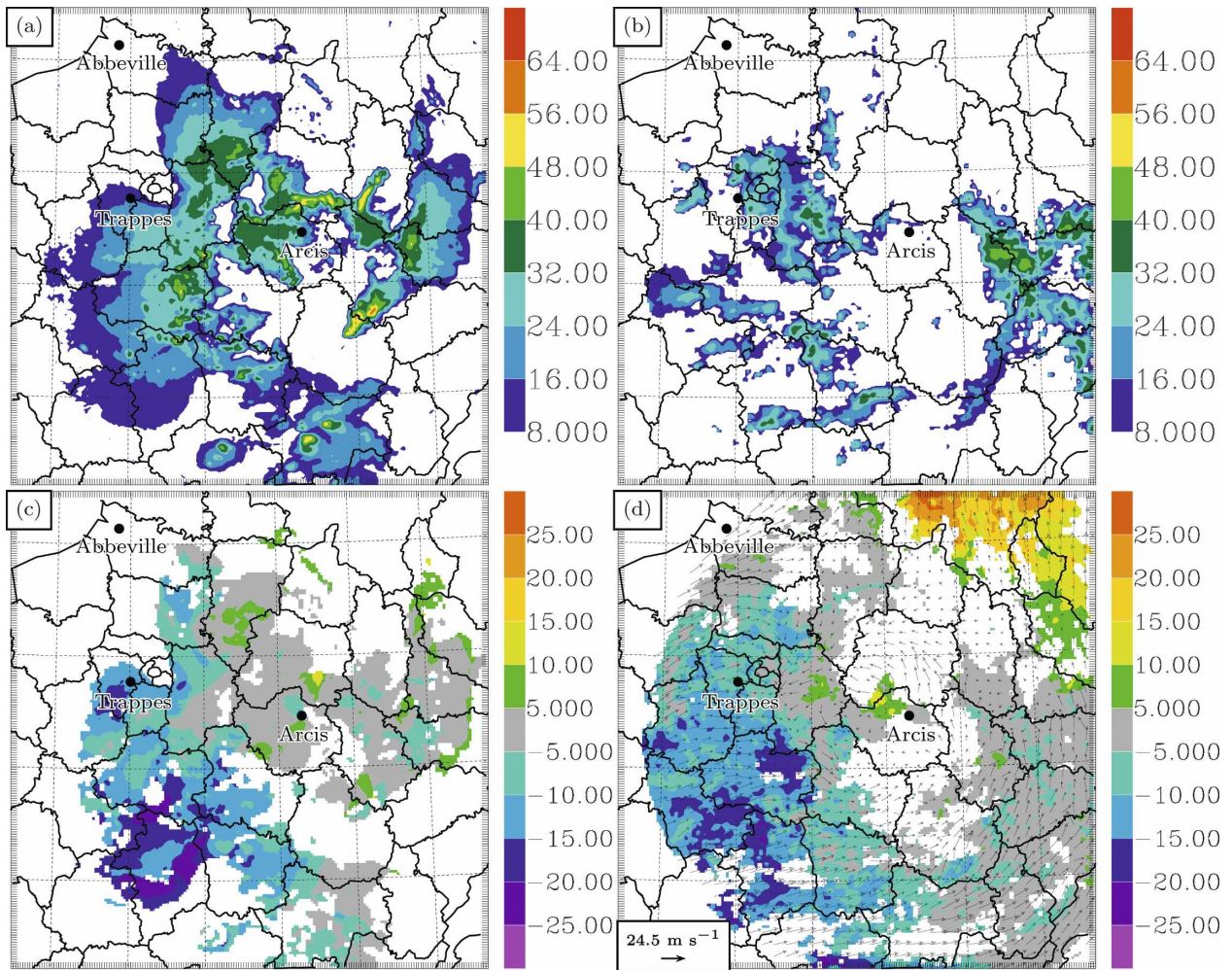
FIG. 1. Reflectivities (dBZ) [(a) observed and (b) simulated] and Doppler radial velocities (m s^{-1}) [(c) observed and (d) simulated] for the Arcis radar at 1800 UTC 23 Jun 2006 at 1.1° elevation. The simulated velocity field on the 1.1°-elevation cone is also plotted in (d). Radial velocities are positive away from and negative toward the radar for all figures.

For this case, Méso-NH produces rainy areas that match roughly the two main active systems visible in the observations in the eastern and western parts of the domain, but the locations and extensions of these areas are not perfect (Figs. 1a,b). In particular, the Méso-NH model tends to underestimate the extensions of stratiform areas (which has already been evidenced in previous studies; e.g., Caumont et al. 2006). As a consequence, there are also some discrepancies between ob-

served and simulated Doppler velocities. However, the general characteristics of the wind fields are captured. The main southwesterly flow southwest of the radar can be very well identified on both observed and simulated Doppler velocities. Note that the area of nonavailable radial velocities (in white) is smaller in the simulation because the threshold for reflectivities is set to a very small value, whereas the real radar system cannot measure correctly Doppler velocities where reflectivities are so small.

3. Sensitivity experiments

The goal of this paper is to assess the impact of using each of three assumptions on the simulated velocities. In the first assumption, the vertical beam broadening is neglected (i.e., velocities are only evaluated at one

TABLE 1. Characteristics of the radars.

	Band	No. of elev	Lowest elev	Highest elev	−3-dB beamwidth
Abbeville	C	2	0.4°	1.1°	1.3°
Arcis	C	5	0.4°	4°	1.1°
Trappes	C	11	0.4°	9.5°	1.1°
Bollène	S	13	0.4°	18°	1.2°

TABLE 2. Characteristics of the sensitivity experiments.

Expt	(1) Vertical broadening neglected	(2) Fall speed neglected	(3) Reflectivity weighting neglected
E_{all}	No	No	No
E_{-vb}	Yes	No	No
E_{-fs}	No	Yes	No
E_{-rw}	No	No	Yes
E_{-vbrw}	Yes	No	Yes
E_{-fsvb}	Yes	Yes	—
E_{-fsrw}	No	Yes	Yes

point for each simulated gate). In this case, Eq. (1) becomes

$$v_r(\mathbf{r}_0) = \frac{\overline{\eta v_r}(\mathbf{r}_0)}{\eta(\mathbf{r}_0)} = u_r(\mathbf{r}_0) - \sin\vartheta \frac{\overline{\eta v_T}(\mathbf{r}_0)}{\eta(\mathbf{r}_0)}, \qquad (2)$$

where ϑ is the elevation of the radar beam,

$$\overline{\eta v_T}(\mathbf{r}_0) = \sum_{j \in \text{type}} \int_0^\infty \sigma_j(D, \mathbf{r}_0) v_{Tj}(D, \mathbf{r}_0) N_j(D, \mathbf{r}_0) \, dD, \tag{3}$$

and v_{Tj} is the fall speed of hydrometeor type j. In the second assumption, hydrometeor fall speeds are neglected. In this case, $v_{rj} = u_r$ and does not depend on D or j. Then,

$$\overline{\eta v_r}(\mathbf{r}) = u_r(\mathbf{r}) \sum_{j \in \text{type}} \int_0^\infty \sigma_j(D, \mathbf{r}) N_j(D, \mathbf{r}) \, dD = \eta(\mathbf{r}) u_r(\mathbf{r}). \tag{4}$$

In the third assumption, the weighting by reflectivities is neglected. In this case, Eq. (1) becomes

$$v_r(\mathbf{r}_0) = \frac{\int_{-\pi}^{\pi} [u_r(\mathbf{r}) - \sin\vartheta \langle v_T \rangle(\mathbf{r})] f^4(\theta) \, d\theta}{\int_{-\pi}^{\pi} f^4(\theta) \, d\theta}, \qquad (5)$$

where

$$\langle v_T \rangle(\mathbf{r}) = \frac{\sum_{j \in \text{type}} \int_0^\infty v_{Tj}(D, \mathbf{r}) N_j(D, \mathbf{r}) \, dD}{\sum_{j \in \text{type}} \int_0^\infty N_j(D, \mathbf{r}) \, dD}. \qquad (6)$$

The first approximation is often assumed because it requires less computer time. The second approximation is used because scanning angles are usually small, which causes the projection of hydrometeor vertical fall speeds onto the beam trajectory also to be small. Atmospheric models, especially those with coarse resolutions, do not always provide hydrometeor fields; in this

TABLE 3. Maximum difference, mean difference, and standard deviation of the difference between the sensitivity experiments and the reference one for Doppler velocities. Results are shown for the Abbeville, Arcis, and Trappes radars between 1500 and 1800 UTC 23 Jun 2005 and for the Bollène radar between 1600 UTC 8 Sep 2002 and 0600 UTC on the day after.

Expt	Δv_{max} (m s^{-1})	Mean diff (m s^{-1})	Std dev (m s^{-1})
	Abbeville		
$E_{-vb} - E_{all}$	29.3	0.11	3.28
$E_{-fs} - E_{all}$	0.33	0.06	0.03
$E_{-rw} - E_{all}$	26.3	0.14	4.58
$E_{-vbrw} - E_{all}$	29.3	−0.02	4.11
$E_{-fsvb} - E_{-fs}$	29.3	0.10	3.28
$E_{-fsrw} - E_{-fs}$	26.3	0.08	4.57
	Arcis		
$E_{-vb} - E_{all}$	−36.4	−0.13	2.83
$E_{-fs} - E_{all}$	0.66	0.08	0.06
$E_{-rw} - E_{all}$	39.6	−0.28	3.76
$E_{-vbrw} - E_{all}$	−36.2	−0.20	3.49
$E_{-fsvb} - E_{-fs}$	−36.4	−0.18	2.52
$E_{-fsrw} - E_{-fs}$	39.5	−0.35	3.75
	Trappes		
$E_{-vb} - E_{all}$	−39.9	0.09	2.76
$E_{-fs} - E_{all}$	1.01	0.08	0.06
$E_{-rw} - E_{all}$	38.0	−0.50	4.23
$E_{-vbrw} - E_{all}$	−39.8	−0.15	3.45
$E_{-fsvb} - E_{-fs}$	−39.9	0.08	2.76
$E_{-fsrw} - E_{-fs}$	−38.1	−0.56	4.23
	Bollène		
$E_{-vb} - E_{all}$	−17.5	−0.15	1.63
$E_{-fs} - E_{all}$	3.22	0.11	0.14
$E_{-rw} - E_{all}$	−26.5	−0.33	2.53
$E_{-vbrw} - E_{all}$	−17.3	−0.21	2.01
$E_{-fsvb} - E_{-fs}$	−19.6	−0.29	2.09
$E_{-fsrw} - E_{-fs}$	−18.4	−0.32	1.96

case, the second and third approximations must be assumed. In addition to the reference simulator configuration presented in section 2b (hereinafter referred to as E_{all}), five sensitivity experiments have been designed in which one, two, or all three assumptions described just above are assumed (Table 2).

About experiment E_{-vb}, one can remark that the weighting by reflectivities only applies to the velocity due to hydrometeor fall speeds [Eq. (2)]. Therefore, experiments neglecting both fall speeds and beam broadening give the same result, regardless of whether the weighting by reflectivities is neglected.

These different types of experiments are applied to the case mentioned in section 2 from 1500 until 1800 UTC and to a flash-flood event that occurred in southern France on 8–9 September 2002 [see Delrieu et al. (2005) for a detailed description] from 1600 until 0600 UTC the day after. For the latter case, data measured by the Bollène radar (see Table 1 for characteristics) are simulated [see Caumont et al. (2006) for the simu-
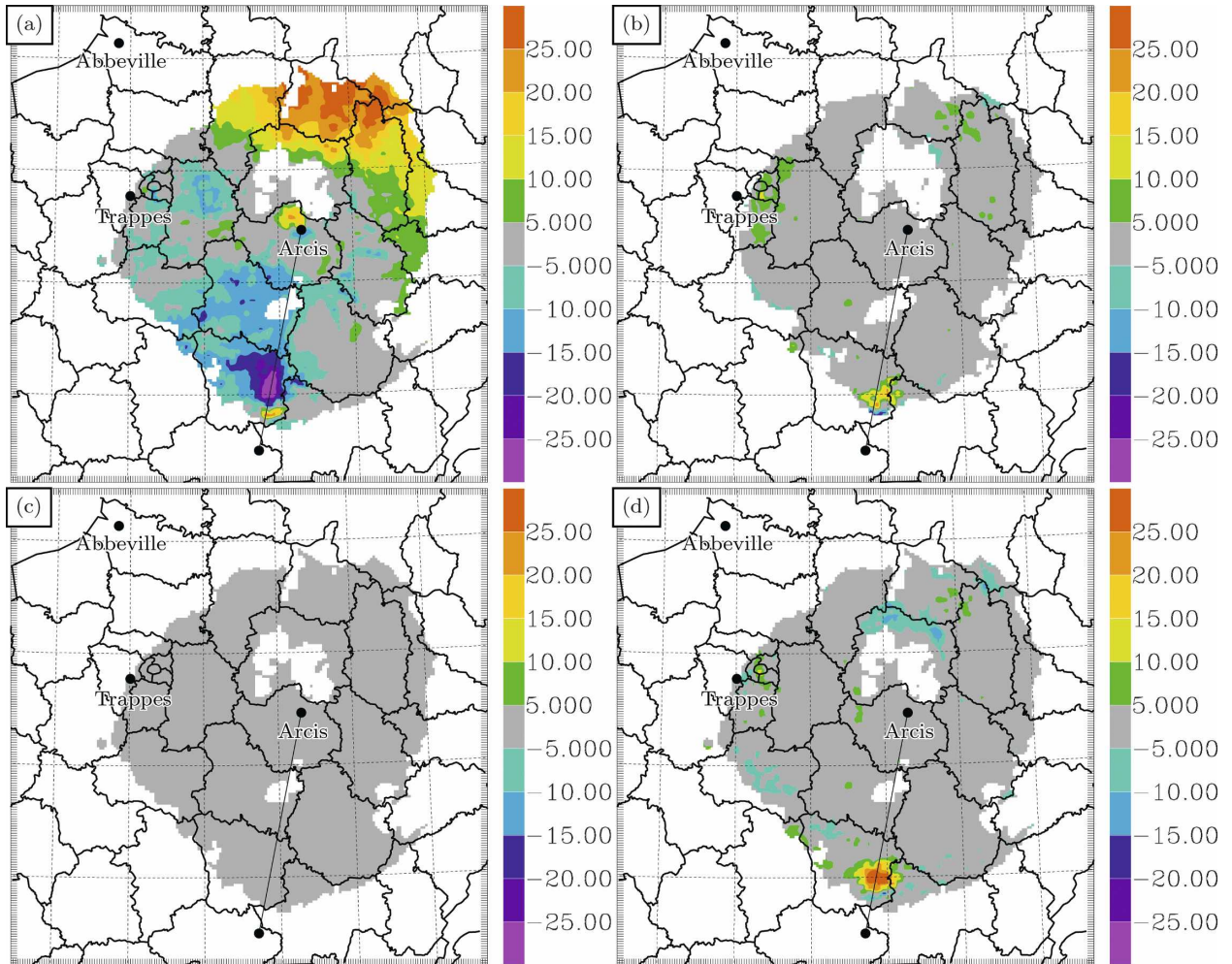
FIG. 2. Simulations of Doppler velocities (m s^{-1}) for the Arcis radar at 1600 UTC 23 Jun 2005, at 4.0° PPI: (a) E_{all}, (b) E_{-vb} − E_{all}, (c) E_{-fs} − E_{all}, and (d) E_{-rw} − E_{all}.

lation of reflectivities]. All radars have a maximum range of 280 km.

4. Results

Departures between the reference experiment and each sensitivity experiment in terms of maximum difference, mean difference, and standard deviation are presented in Table 3 for the two simulations. For each radar, these statistics are computed for all elevations, every hour of simulation, wherever data can be simulated.

Table 3 shows that neglecting fall speeds (E_{-fs} vs E_{all}) does not impact significantly the accuracy of the results considering our radar configuration (i.e., maximum elevation of 18°). It can also be seen that E_{-vb}, E_{-rw}, and E_{-vbrw} all depart from E_{all} by similar magnitudes. On average, neglecting the weighting by reflec-

tivities (E_{-rw}) brings the largest difference in comparison with the reference experiment (E_{all}). This feature means that errors resulting from neglecting the vertical beam broadening and the weighting by reflectivities are not additive. Note that this conclusion also holds true when hydrometeor fall speeds are already neglected (i.e., when the reference simulation is E_{-fs} instead of E_{all}): in Table 3, the differences between E_{-fsvb} and E_{-fs} are similar to those between E_{-fsrw} and E_{-fs}.

The high values for maximum differences mainly occur at distant range gates because of heterogeneities within beam gates. To illustrate this, we give a closer look at a typical 4.0° PPI of Doppler velocities simulated for the Arcis radar, for which particularly large discrepancies between the reference experiment and other experiments are found (Fig. 2). The largest discrepancies between the reference simulation and that without reflectivity weighting or without beam broad-
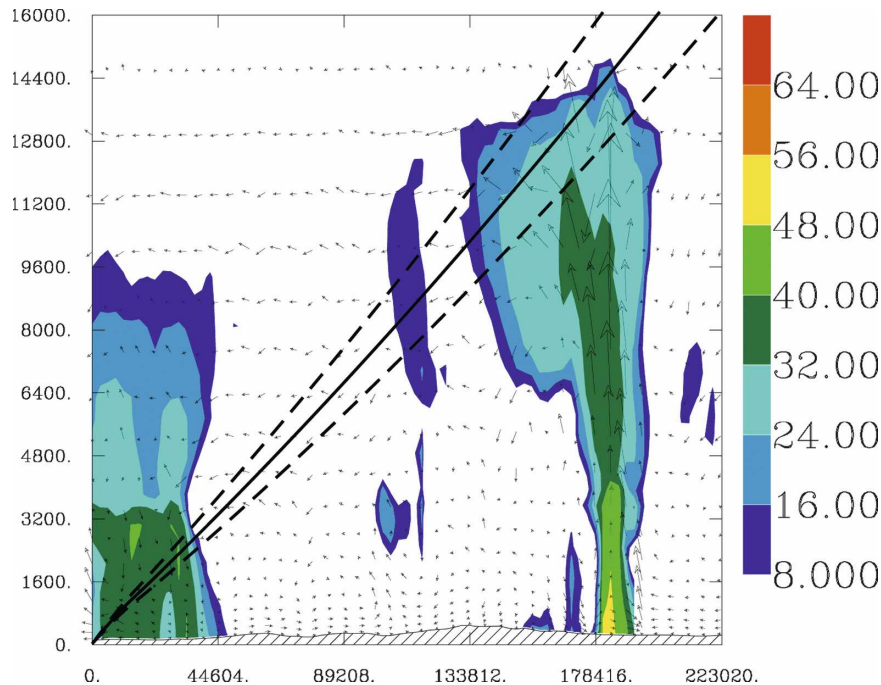
FIG. 3. Vertical cross section of simulated reflectivities (dBZ) between the two points in Fig. 2 for the Arcis radar at 1600 UTC 23 Jun 2005. The Arcis radar is located at the bottom-left of the figure. The solid line represents the 4.0°-elevation ray path; the dashed lines represent the −3-dB beam contours.

ening are located south of the radar. This area is related to a convective cell and, in particular, to the anvil of this convective cell (Fig. 3). The main vertical updraft of this convective cell, with maximum speeds of 20 m s^{-1}, is blocked by the tropopause, and the wind becomes divergent to form the anvil. Thus, there are relatively high horizontal speeds near the tropopause, whereas the winds are mainly vertical in the updraft below. The reflectivities are high within the updraft (many condensed hydrometeors including graupel), whereas they are low in the anvil (mainly snow and primary ice). At this range, the radar beam encompasses a large area with strong heterogeneities, both in wind speeds and reflectivities. In the reference simulation (Fig. 2a), radial velocities become more negative as they get closer to the convective cell and then become positive behind the convective core because of the divergent wind flow in the anvil.

For the simulation without beam broadening (cf. Fig. 2b), the discrepancies in this area are explained by the fact that radial velocities are only evaluated along the solid line in Fig. 3. Thus, radial velocities become more negative as they approach the convective cell (as in the reference simulation), but the southern part of the anvil with positive radials velocities is missed (it is overshot by the solid line). The negative values ahead of the

convective core are less negative in this simulation because the maximum negative wind speeds at the bottom of the beam, (i.e., in the updraft, where reflectivities are highest) are not taken into account.

For the simulation without weighting by reflectivities (cf. Fig. 2d), negative radial velocities ahead of the convective core are closer to zero than in the reference simulation because they are less weighted toward the maximum negative wind speeds located in the updraft, where reflectivities are also maximum. In the southern part of the convective cell, the top of the anvil with negative radial velocities receives the same weight as the positive radial velocities located below in the vicinity of the updraft. In the reference simulation, the positive radial velocities receive more weight because they are associated with higher reflectivities. That is why the area of positive radial velocities in the reference simulation is not reproduced in the simulation without weighting by reflectivities.

5. Conclusions

We have simulated Doppler velocities from a high-resolution atmospheric model with simulators accounting for or neglecting the following physical processes: hydrometeor fall speeds, vertical broadening of the radar beam with range, and weighting of velocities by

reflectivities. We conclude that neglecting the particle fall speeds does not importantly affect the estimation of Doppler velocities in comparison with neglecting the beam broadening or the weighting by reflectivities, as long as the elevation angle remains low (18° maximum in our study).

The larger errors caused by neglecting the beam broadening or the weighting by reflectivities are due to heterogeneities in wind speed and reflectivity in farther gates. It was shown above that such heterogeneities can appear in convective cell anvils and lead to larger inaccuracies in the estimation of Doppler velocities when the beam broadening or the weighting by reflectivities (or both) is neglected.

Note also that neglecting both the beam broadening and the weighting by reflectivities (experiment $E_{-\mathrm{vbrw}}$) does not have an additive impact on error statistics. In fact, all error statistics for this experiment do not exceed those of experiments $E_{-\mathrm{vb}}$ and $E_{-\mathrm{rw}}$. It can be concluded that accounting only for either beam broadening or weighting by reflectivities does not much improve the accuracy of simulated Doppler velocities in comparison with neglecting both effects. In converse, this accuracy is much improved when both effects are taken into account.

This study only focused on a specific number of errors caused by some simplifications in the design of radar simulators. Because the reference simulation, which takes into account all three effects discussed in this paper, contains some simplifications itself (standard curvatures for beam paths, no attenuation, etc.), errors computed in this paper associated with some simplification might be larger in reality (i.e., in comparison with a reference simulation that could account for *all* errors).

REFERENCES

Caniaux, G., J.-L. Redelsperger, and J.-P. Lafore, 1994: A numerical study of the stratiform region of a fast-moving squall line. Part I: General description and water and heat budgets. *J. Atmos. Sci.,* **51,** 2046–2074.

Caumont, O., and Coauthors, 2006: A radar simulator for high-resolution nonhydrostatic models. *J. Atmos. Oceanic Technol.,* **23,** 1049–1067.

Cheong, B. L., R. D. Palmer, and M. Xue, 2008: A time series weather radar simulator based on high-resolution atmospheric models. *J. Atmos. Oceanic Technol.,* **25,** 230–243.

Delrieu, G., and Coauthors, 2005: The catastrophic flash-flood event of 8–9 September 2002 in the Gard region, France: A first case study for the Cévennes–Vivarais Mediterranean Hydrometeorological Observatory. *J. Hydrometeor.,* **6,** 34–52.

Doviak, R. J., and D. S. Zrnić, 1993: *Doppler Radar and Weather Observations.* 2nd ed. Academic Press, 562 pp.

Ducrocq, V., D. Ricard, J.-P. Lafore, and F. Orain, 2002: Storm-scale numerical rainfall prediction for five precipitating events over France: On the importance of the initial humidity field. *Wea. Forecasting,* **17,** 1236–1256.

Lafore, J.-P., and Coauthors, 1998: The Meso-NH Atmospheric Simulation System. Part I: Adiabatic formulation and control simulations. *Ann. Geophys.,* **16,** 90–109.

May, R. M., M. I. Biggerstaff, and M. Xue, 2007: A Doppler radar emulator with an application to the detectability of tornadic signatures. *J. Atmos. Oceanic Technol.,* **24,** 1973–1996.

Qiu, C.-J., A.-M. Shao, S. Liu, and Q. Xu, 2006: A two-step variational method for three-dimensional wind retrieval from single Doppler radar. *Meteor. Atmos. Phys.,* **91,** 1–8, doi:10.1007/s00703-004-0093-8.

Salonen, K., and H. Järvinen, 2004: The fit of Doppler radar radial winds with the NWP model counterpart. *Proc. Third European Conf. on Radar in Meteorology and Hydrology,* Visby, Sweden, Copernicus Gesellschaft, 469–473.

Snyder, C., and F. Zhang, 2003: Assimilation of simulated Doppler radar observations with an ensemble Kalman filter. *Mon. Wea. Rev.,* **131,** 1663–1677.

Sun, J., and N. A. Crook, 1997: Dynamical and microphysical retrieval from Doppler radar observations using a cloud model and its adjoint. Part I: Model development and simulated data experiments. *J. Atmos. Sci.,* **54,** 1642–1661.

——, and ——, 2001: Real-time low-level wind and temperature analysis using single WSR-88D data. *Wea. Forecasting,* **16,** 117–132.

Tong, M., and M. Xue, 2008: Simultaneous estimation of microphysical parameters and atmospheric state with simulated radar data and ensemble square root Kalman filter. Part I: Sensitivity analysis and parameter identifiability. *Mon. Wea. Rev.,* **136,** 1630–1648

Wu, B., J. Verlinde, and J. Sun, 2000: Dynamical and microphysical retrievals from Doppler radar observations of a deep convective cloud. *J. Atmos. Sci.,* **57,** 262–283.

Xue, M., M. Tong, and K. K. Droegemeier, 2006: An OSSE framework based on the ensemble square root Kalman filter for evaluating the impact of data from radar networks on thunderstorm analysis and forecasting. *J. Atmos. Oceanic Technol.,* **23,** 46–66.